CONF-910435--30

SAND--90-7059C

DE91 005966

SAND90-7059C

Effect of a Low-Permeability Layer on Calculated Gas Flow at Yucca Mountain

Ning Lu, Steven Amter, Benjamin Ross
Disposal Safety Inc., Washington, DC

The analyses for this document were gathered under Quality Assurance Level NQ, WBS 1.2.1.4.1.

SAND 90-7054C
final draft
12/5/90

EFFECT OF A LOW-PERMEABILITY LAYER ON CALCULATED GAS FLOW AT YUCCA MOUNTAIN*

Ning Lu
Steven Amter
Benjamin Ross

Disposal Safety Incorporated
1660 L Street NW, Suite 314
Washington, DC 20036

INTRODUCTION

Yucca Mountain is being studied to determine its suitability as a location for a high-level nuclear waste repository. The mountain is a steep-sided linear ridge which is underlain by a 500-meter thick unsaturated zone composed of alternating layers of ash-flow and bedded tuffs.[1]

Seasonal flows of air with velocities as high as 3.5 m/s have been observed[2] in deep boreholes at Yucca Mountain. These flows are attributed to convective circulation arising from topographic relief, seasonal temperature variation, and density differences resulting from variation in gas composition. If a repository were built there, heat from the emplaced waste would also contribute to gas flow. Large-scale air flows may be significant to repository performance because they control the movement of carbon dioxide within the mountain and also result in a net flux of water vapor to the surrounding atmosphere. An understanding of the velocity, trajectories, and mixing of the gas in Yucca Mountain is necessary both as input for a model of the carbon-14 movement in the unsaturated zone[3] and evaluation of the net vapor flux.

Amter and Ross[4] developed a model called TGIF (Topographic Induced Flow) to simulate gas flow under Yucca Mountain. The TGIF model differs significantly from previous gas flow models. It uses a governing equation that is based on the concept of freshwater head, thus avoiding the numerical problems associated with the near-cancellation of the forces due to gravity and the pressure gradient. Unlike most other models, dipping, layered media can be simulated.

This paper describes a systematic sensitivity study that was designed to test several aspects of the TGIF model when used to simulate gas flow under Yucca Mountain. Values of three important inputs to the model were systematically varied to form a matrix of 80 runs. The matrix consisted of five values of permeability contrast between a bedded tuff layer and surrounding welded units (in all cases, bulk permeabilities were used to represent the combined effect of both fractures and matrix permeability), four temperature profiles representing different stages of repository cooldown, and four finite-difference grids.

THE MODEL

The derivation of the governing equation on which TGIF is based involves the following assumptions about the physical system in the deep subsurface at Yucca Mountain:

- Thermodynamic equilibrium exists between air, water vapor, and water.
- The gas behaves as an ideal gas.
- The gas is saturated with water vapor.
- The gas flow field is at steady state.
- Changes in partial pressure of water vapor are accommodated by changes in gas composition, with the total pressure remaining nearly constant.[5]
- Gas viscosity is independent of pressure.
- Acceleration of gravity is uniform.
- Molecular diffusion resulting from gradients of water vapor partial pressure has a negligible effect on gas flow.[4]
- All gas-filled voids in the matrix may be treated as a single porosity on time scales of years. (see data of Montazer et al.[6]).

* This work was performed under the auspices of the U.S. Department of Energy, Office of Civilian Radioactive Waste Management, Yucca Mountain Project, under Contract DE-AC04-76DP00789

- Gas permeability is independent of pressure.
- The unsaturated zone stays at constant saturation, with water lost to evaporation replenished by precipitation or from the water table.

The validity of these assumptions at sufficiently low temperatures is well established. They imply that the system can be described by three equations, a volume balance, a constitutive relation, and Darcy's Law, as follow:

$$\nabla\cdot q - q\left[\left(\frac{1}{T}+\frac{1}{P_a}\frac{dP_v}{dT}\right)-\frac{1}{P_a}\nabla P\right] = 0 \qquad (1)$$

$$\rho=\frac{1}{RT}(P_v\Omega_v+P_a\Omega_a) \qquad (2)$$

$$q=-\frac{K}{\mu}(\nabla P-g\rho\hat{z}) \qquad (3)$$

where q is the volumetric flux of gas (or Darcy velocity), T is the temperature, P is the pressure, P_v is the vapor pressure of water, P_a is defined by $P_a = P-P_v$, ρ is the gas density, R is the gas constant, Ω_a and Ω_v are the molar weights of dry air and water, K is the permeability of the rock, μ is the viscosity of the gas, g is the acceleration of gravity, and $\hat{z}$ is a downward-pointing unit vector. To avoid the numerical problems associated with the subtraction of two large numbers to yield a small number, Amter and Ross[4] recast the problem in terms of a variable h (called "the freshwater head") defined by

$$h=\frac{P-P_o}{g\rho_o}-z \qquad (4)$$

where P_o and ρ_o are reference values of pressure and density. The governing equation then is approximated as:

$$\nabla^2 h - m\nabla T\cdot\nabla h+\left[\frac{1}{T}+g\frac{\Omega_a-\Omega_v}{RT}\frac{dh_v}{dT}+\rho'\left(\frac{1}{T}+m\right)\right]\frac{\partial T}{\partial z} - \frac{g\Omega_a}{RT}-\frac{\rho'}{h_a} = 0 \qquad (5)$$

where

$$m=\frac{1}{\mu_o}\frac{d\mu}{dT}\Big|_{T_o}+\frac{1}{h_a}\frac{dh_v}{dT}+\frac{1}{T_o} \qquad (6)$$

$$\rho'=\frac{\rho}{\rho_o}-1 \qquad (7)$$

and h_a and h_v are related to P_a and P_v by (4).

A new addition to TGIF is a post-processor particle tracker, which facilitates the direct generation of gas particle path lines. The particle tracker is based on the theory developed by Pollock[7], with modifications for use with a node-centered flow model.

PHYSICAL PROPERTIES OF THE SYSTEM

Gas flow was simulated in a two-dimensional vertical section that cuts across the south portion of Yucca Mountain where a nuclear waste repository might be located. A schematic of the simulated section is shown in Figure 1.

The mountain contains a number of hydrostratigraphic subdivisions of the Paintbrush Tuff Formation. These layers dip approximately six degrees to the east and differ in permeability. The most important hydrostratigraphic feature of the modeled section is a thin, nonwelded tuff layer which includes all or part of several stratigraphic subdivisions of the Paintbrush Tuff.[1] This unit, the Paintbrush nonwelded unit, is sparsely fractured and thus is thought to have a relatively lower permeability. It lies between two thick, welded, densely fractured, and relatively permeable units, the Tiva Canyon welded unit (above) and the Topopah Spring welded unit (below).

A permeability of 10^{-11} m^2 is used for both the Tiva Canyon unit and the Topopah Spring unit while permeabilities of 10^{-14}, 10^{-13}, 10^{-12}, 10^{-11}, and 10^{-10} m^2 are used for the nonwelded unit in the simulations. Since the path lines depend only on the degree of the permeability contrast between the two kinds of tuff and not on the absolute magnitude of the permeability, travel times for other values of welded-tuff permeability can be obtained from travel times reported here by dividing by the ratio of the permeabilities.

The simulation region is surrounded by two types of boundary conditions (Figure 1),

- the mountain's atmospheric contact along its surface, and
- no-flow conditions along the base and sides.

The no-flow boundary assigned at the base of the simulated region represents the top of the low-permeability tuffaceous beds of the Calico Hills unit, which would impede downward gas flow. The boundary to the west is located in the trough of Solitario Wash, which is a natural flow divide. The third no-flow boundary is located far enough to the east to have little effect on flow near the repository, as shown by additional simulations not reported here. Numbers shown in Figure 1 represent starting locations of particle tracks.

The four temperature fields were calculated using Laplace's equation and prescribed temperatures at the repository and all boundaries. Along the atmospheric boundary, a uniform temperature (independent of elevation) was assumed based on an assumed annual average. Temperatures at the base of the cross-section

varied with elevation, following an assumed geothermal gradient.

SIMULATIONS

A matrix of 80 simulations was constructed by varying three important aspects of the simulation (see Figure 2). These were:

- the temperature of the repository and surrounding rock,
- the permeability of the Paintbrush nonwelded unit, which is the middle layer in the simulation, and
- nodal density used to represent the Paintbrush nonwelded unit and also the entire simulation.

The entire three-dimensional matrix of simulations is shown schematically in Figure 2, where K is the intrinsic permeability of the Paintbrush nonwelded unit and K' is the intrinsic permeability of the surrounding Tiva Canyon and Topopah Spring welded units.

Five different permeability contrasts were used in the simulations. The Paintbrush nonwelded unit was assumed to be 10 times more permeable and also 1, 10, 100, and 1000 times less permeable than the surrounding welded units, which were assigned a permeability of 10^{-11} m^2. The objective was to test the model over the range of contrasts that was found by Montazer et al.[6]

As depicted in Figure 2, the matrix of simulations included four different assumed temperature profiles.[4] The ambient condition represents the current condition of a linear geothermal gradient of 2.0 K per 100 m. In the remaining three situations, the subsurface was assumed to have been heated by the nuclear waste in the repository, raising temperatures 3, 14, and 30 K over ambient conditions. Although these are temperatures that might be expected thousands, tens of thousands, or perhaps hundreds of thousands of years from now, future repository temperatures are uncertain, and these simulations are not intended as predictions of conditions at any particular time. Rather, this range in temperatures was used to examine how gas flow may be affected by temperature.

To examine the sensitivity of the model to mesh density, the number of rows used in the simulation, particularly in and around the middle layer, was varied. Four different meshes were employed.

The first mesh contained 12 rows and 46 columns of blocks. The middle layer contained three rows of rectangular blocks that measured 20 m (vertical length) by 40 m. The remaining blocks were squares with sides of 40 m.

In the second mesh, the number of rows and columns was doubled to 25 and 92. This resulted in a mesh consisting entirely of square blocks that measured 20 m on a side. As in the first case, three rows of blocks were used to represent the Paintbrush nonwelded unit.

The third mesh was a modification of the second mesh. The number of rows of blocks used to represent the Paintbrush nonwelded unit was increased from three to five by decreasing by half the row spacing in the middle unit. The Paintbrush nonwelded unit was thus represented by 4 rows of rectangular blocks that measured 10 m by 20 m. The rest of the domain retained square blocks.

The fourth mesh was also a modification of the second mesh. The number of rows of blocks was increased to 32 by halving the row spacing not only in the Paintbrush nonwelded unit, but also four blocks into the surrounding units. This mesh, shown in Figure 3, contained 12 rows of blocks measuring 10 m by 20 m, 4 of which represented the Paintbrush nonwelded unit. The rest of the mesh retained square blocks.

RESULTS

The results of the 80 simulations demonstrate that the predicted pattern of flow is highly dependent on the temperature and permeability contrast. Selected output from the model, in the form of particle tracks, illustrates the major trends.

The Effect of Temperature

The temperature of the repository affects both the velocity of gas particles leaving the repository and the direction of the path lines. Figures 4a-c show the path lines for simulations in a uniform medium (no permeability contrast) at ambient conditions and repository temperatures of 314 K and 330 K.

As the repository temperature increases, the vertical velocity component for gas particles exiting from the repository also increases. Increasing temperature thus decreases path-line curvature and length and also decreases transit times for particles traveling from the repository to the atmosphere. Figure 5 shows how the shortest particle travel time from the repository to the surface is related to the repository temperature. In all simulations, particles starting from near the left end of the repository had the shortest travel time. Since the contrast between the permeability of the middle and surrounding layers also affects travel time, curves corresponding to five different permeability contrasts are shown.

The Effect of Permeability Contrast

The degree to which the permeability of the middle unit differs from the surrounding layers has a pronounced effect on the flow system predicted by the TGIF model. When a particle crosses a permeability boundary, its trajectory appears to follow the law of tangents, as one would expect. In addition, temperature

and tilting of the layers affect the pattern of gas flow. With sufficient permeability contrast, the middle layer acts as a true confining layer, with independent flow systems above and below it.

Low-temperature situation Figures 6a-e show path lines with the ambient temperature profile (no repository heating) and five different contrasts in permeability. In Figure 6b, the uniform permeability case, the path lines are smooth, are nearly symmetric around the center of the mountain, and all exit near the crest of the mountain. Figure 6a shows the case where the middle layer is 10 times more permeable than the surrounding layers. As would be expected, refraction in the direction of the bedding plane causes greater convergence of the flow lines. Figures 6c-e show that when the middle layer has a progressively smaller permeability, the Paintbrush nonwelded unit becomes an increasingly effective confining layer. In Figure 6c (middle layer 10 times less permeable), path lines are refracted perpendicular to the bedding plane, reducing the convergence of the path lines. In Figure 6d (permeability 100 times less), path lines are diverted some distance laterally outward beneath the middle layer before penetrating it and traveling to the surface. Note that there is a pronounced convergence of these path lines above the layer. At a permeability contrast of a thousand, shown in Figure 6e, confinement by the middle layer is nearly complete; only one gas particle penetrates the layer. Path lines originating from the left side of the repository are directed laterally beneath the middle layer until they exit at the atmospheric boundary. Path lines under the layer from the center and right side of the repository form a convection cell driven by a small horizontal temperature gradient. (When the temperature boundary conditions are changed slightly to eliminate the horizontal gradient, the convection cell disappears.)

High-temperature situation Figures 7a-e show the path lines from a repository heated at a temperature of 330 K with five different contrasts in permeability. Although refraction again occurs in the middle layer, there are some important differences from the low temperature situation. Because the higher temperature causes a stronger buoyant flow, path lines tend to be shorter and more vertical when the permeability contrast is relatively small. This can be seen in Figures 7a-b. However, the higher velocities also promote divergent flow beneath the middle layer and the formation of convection cells at both ends of the repository as the permeability contrast increases (Figures 7c-e). When the permeability contrast reaches a factor of 1000 (Figure 7e), the middle layer becomes an effective confining layer and no path lines penetrate it.

Development of an upper and lower flow system As the permeability contrast increases, there is an increased tendency toward the development of separate flow systems on either side of the middle layer. This can be seen by comparing Figures 4c and 7e. In the no-contrast, high temperature case depicted in Figure 4c, the mountain contains a single flow system with a simple pattern of circulation. Some of the air entering the mountain flows deep enough to pass through the repository. All path lines originating from the repository exit near the crest of the mountain.

A very different situation can be seen in Figure 7e, which depicts the high contrast, high temperature case. Completely separate flow systems form above and below the middle layer because gas particles cannot penetrate it. Circulation in the upper system is very shallow and exits at the mountain's crest. In the lower flow system, gas particles from the left portion of the repository exit the left slope of the mountain where the lower layer crops out. Gas particles released from the right portion of the repository circulate back on themselves.

Travel Times Despite the thinness of the Paintbrush nonwelded unit, its permeability has a significant affect on the time required for gas particles originating from the repository to exit the mountain. Travel times generally increase as the permeability of the Paintbrush nonwelded unit decreases. However, reducing the permeability by three orders of magnitude only increases the travel time by one order of magnitude. The reduction in travel times arises from two causes: decreased velocities through the layer and longer path lengths due to refraction. Figure 8 shows the relationship between permeability contrast and the minimum travel time for four different repository temperatures. Up to a permeability contrast of 100 times, there is a steady rise in travel time. An interesting exception to the trend occurs when the permeability contrast is 1000 times. Travel times for particles originating from the left side of the repository decrease because diversion beneath the middle layer causes path lengths to shorten. Examples of this can be seen in Figures 6e and 7e.

The Effect of Mesh Density

Varying the mesh density produces only minor changes in predicted gas path lines. This can be seen in Figure 9, which shows path lines for three different mesh densities when the repository temperature is 303 K and the permeability contrast is 10 times. The predicted path lines for particles released from the repository are very similar for the three different mesh densities. In fact, at the left side of the repository the path lines are virtually indistinguishable. This is also the case for path lines originating from positions 2 through 6. The fact that the path lines are relatively insensitive to the changes in the mesh density indicates that all meshes used in this study are fine enough to yield reasonable results.

CONCLUSIONS

The TGIF model appears to be capable of simulating gas flow at Yucca Mountain over a wide range of inputs. Gas-flow path lines and travel times are highly

dependent on the repository temperature as well as the degree of contrast between the Paintbrush nonwelded unit and surrounding layers. At extremely high permeability contrasts, two independent flow systems form above and below the middle layer.

The model can be used to calculate unretarded gas particle travel times in Yucca Mountain. By accounting for retardation, carbon-14 travel time could also be calculated. If the predicted travel time is less than 10,000 years, then more detailed analysis will have to be considered to determine compliance with proposed EPA regulations. Such analysis may require additional, more definitive data describing permeabilities in the mountain. Other parameters, such as waste-package performance, may also need to be considered.

REFERENCES

(1) Scott, R.B., and J. Bonk, 1984. "Preliminary Geologic Map of Yucca Mountain, Nye County, Nevada, with Geologic Sections," U.S. Geological Survey Open-File Report 84-494, Denver, CO.

(2) Weeks, E.P., 1987. "Effect of Topography on Gas Flow in Unsaturated Fractured Rock--Concepts and Observations," *Flow and Transport Through Unsaturated Fractured Rock*, edited by D.D. Evans and T.J. Nicholson, Geophysical Monograph 42, American Geophysical Union, pp. 165-170.

(3) Ross, B., 1988. "Gas-Phase Transport of Carbon-14 Released From Nuclear Waste into the Unsaturated Zone," *Scientific Basis for Nuclear Waste Management XI*," edited by M.J. Apted and R.E. Westerman, Materials Research Society, Pittsburgh, pp. 273-284.

(4) Amter, S. and B. Ross, 1990. "Simulation of Gas Flow Beneath Yucca Mountain, Nevada, with a Model Based on Freshwater Head," *Proceedings of the Symposium on Waste Management*, edited by R.G. Post, Tucson AZ, vol. 2, pp. 915-925.

(5) Ross, B., 1984. "A Conceptual Model of Deep Unsaturated Zones With Negligible Recharge", *Water Resour. Res.*, vol. 20, pp. 1627-1629.

(6) Montazer, P., E.P. Weeks, F. Thamir, S.M. Yard, and P.B. Hofrichter, 1985. "Monitoring the Vadose Zone in Fractured Tuff, Yucca Mountain, Nevada," *Proceedings of the NWWA Conference on Characterization and Monitoring of the Vadose (Unsaturated) Zone*, Denver, pp. 439-469.

(7) Pollock, D.W., 1988. "Semi-Analytical Computation of Path Lines for Finite-Difference Models," *Ground Water*, vol. 26, pp. 743-750.

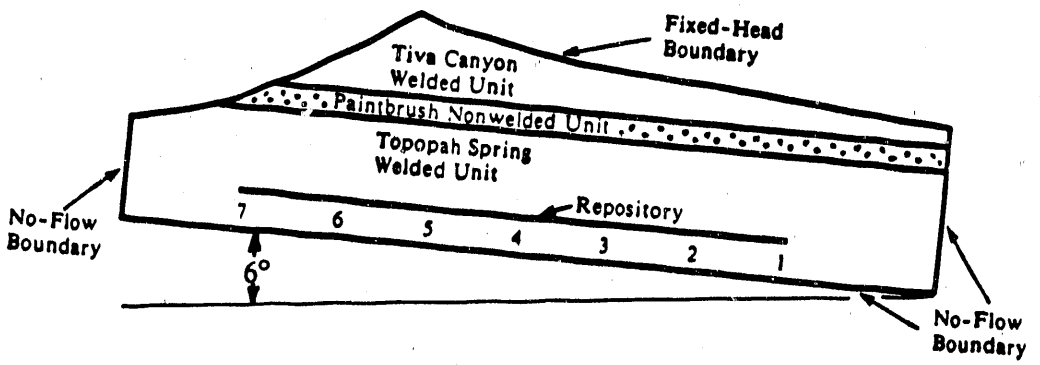

Figure 1. Geometry of cross section used in the gas flow simulation.

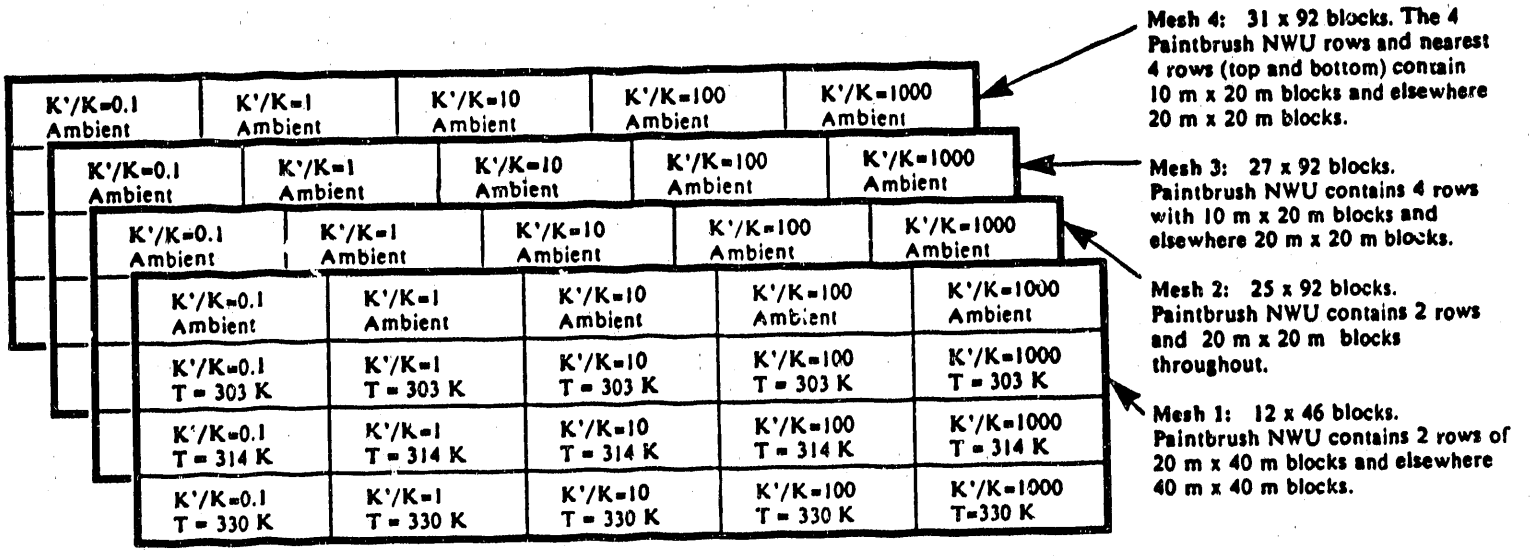

Figure 2. Matrix of simulation cases.

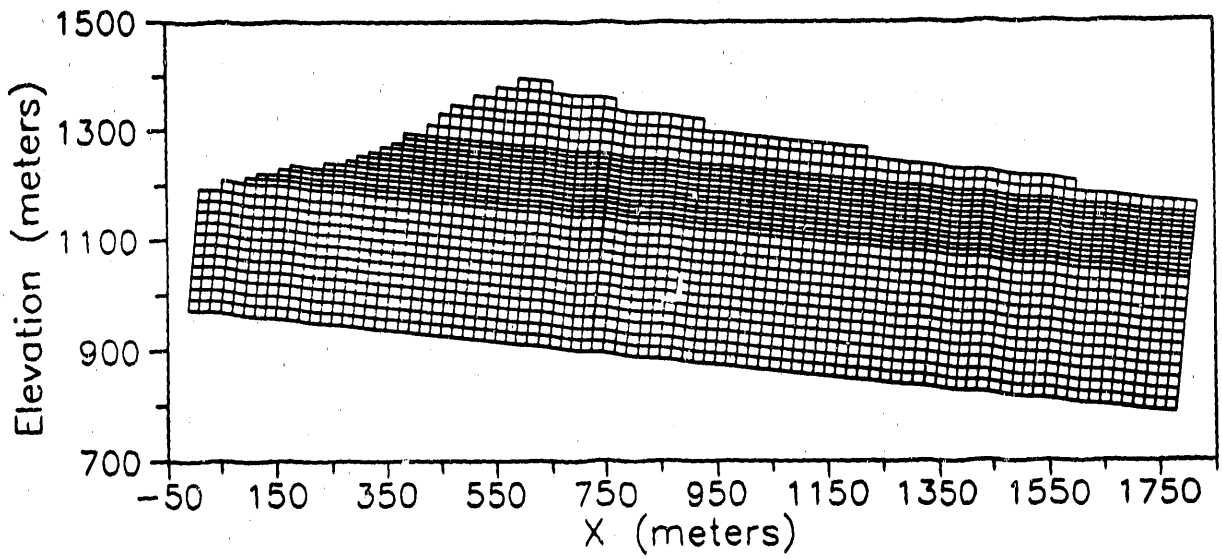

Figure 3. Two-dimensional finite difference grid (31 x 92 blocks).

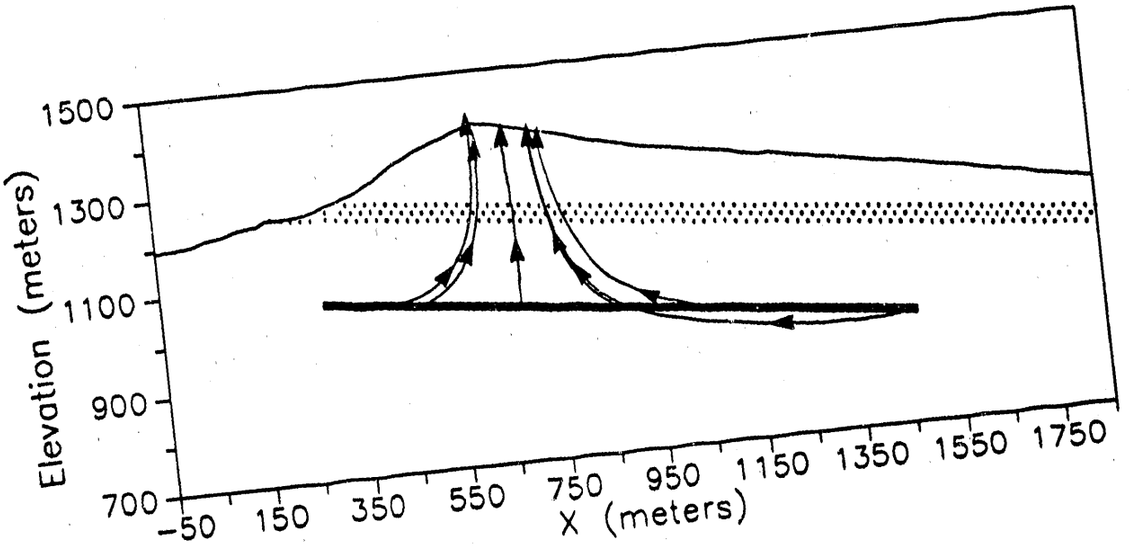

Figure 4a. Path lines with ambient temperature, no permeability contrast.

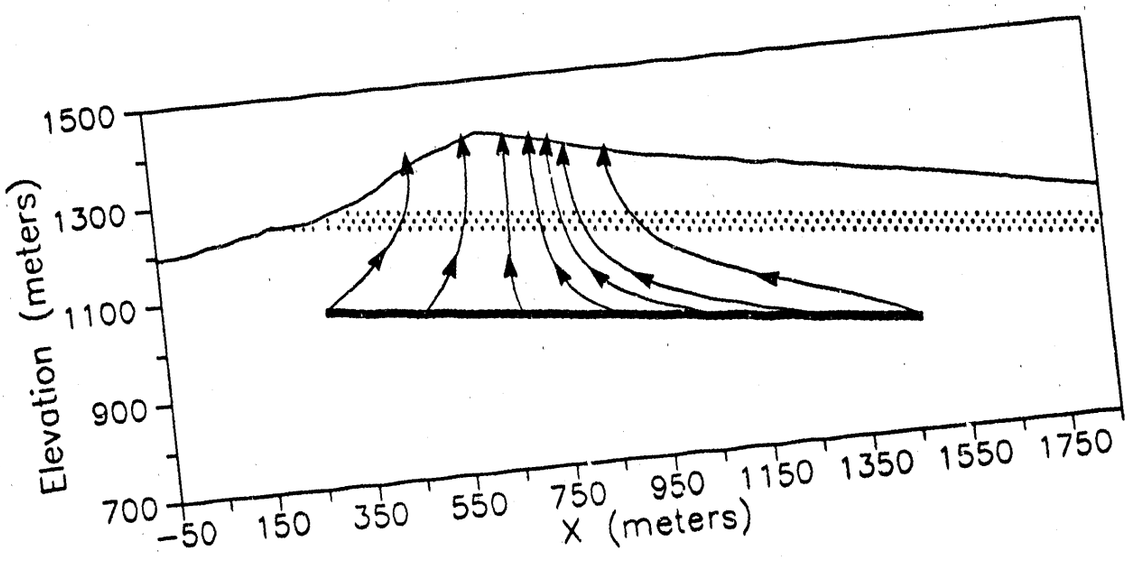

Figure 4b. Path lines with the repository heated to 314 K, no permeability contrast.

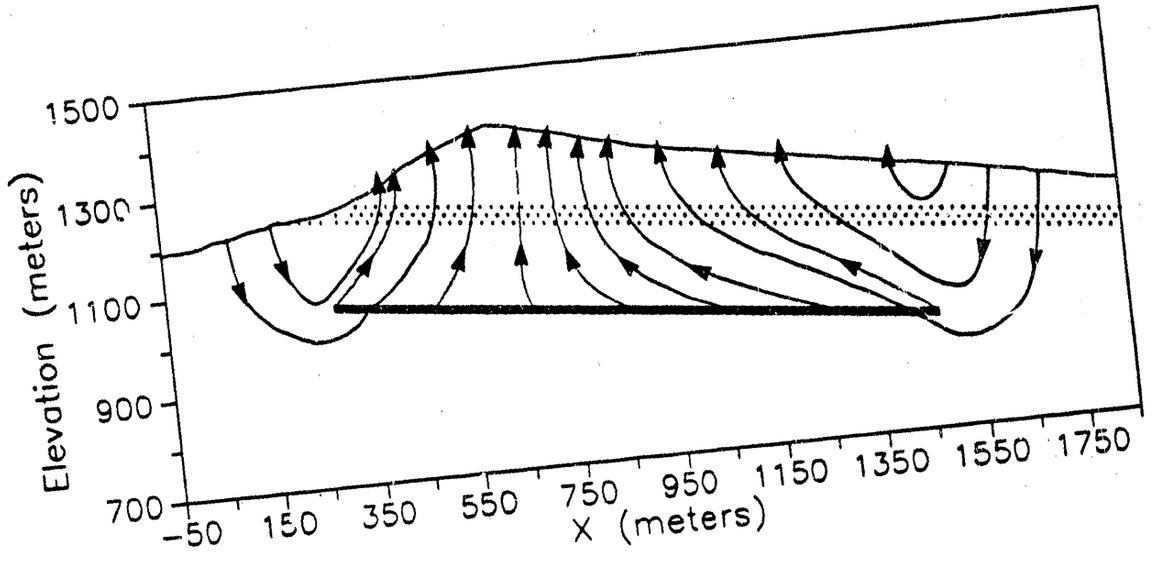

Figure 4c. Path lines with the repository heated to 330 K, no permeability contrast.

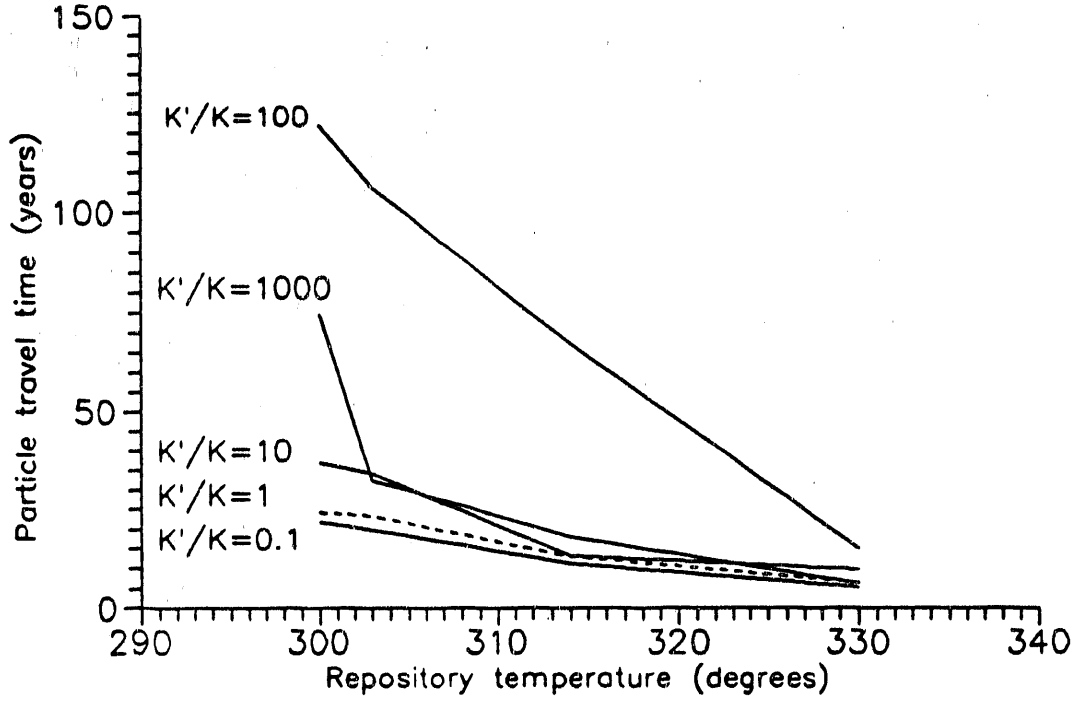

Figure 5. The minimum particle travel time from the repository as a function of temperature at the repository.

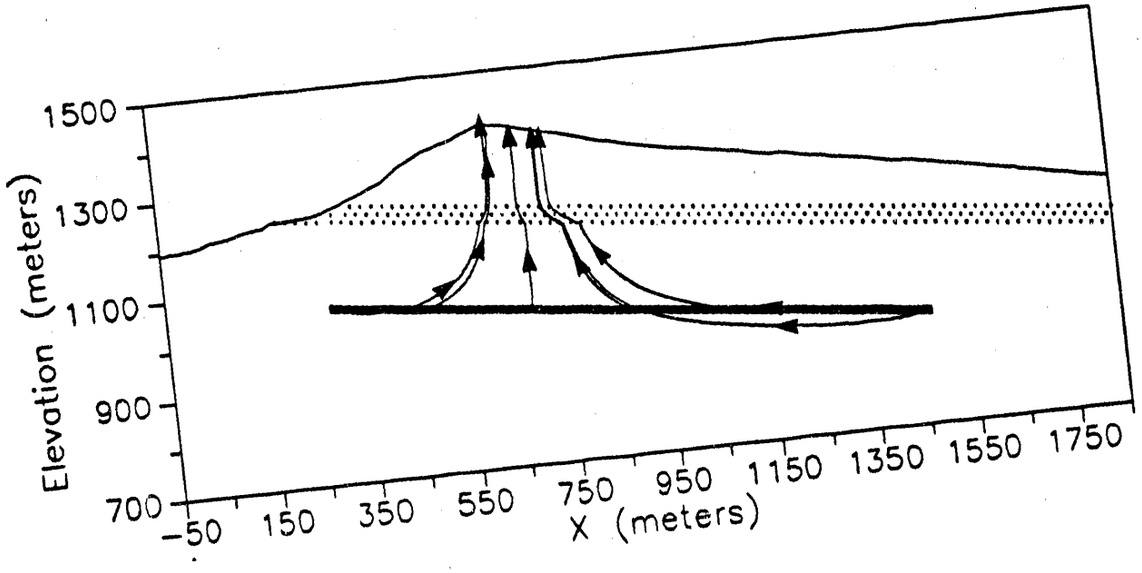

Figure 6a. Path lines with ambient temperature, 0.1× permeability contrast.

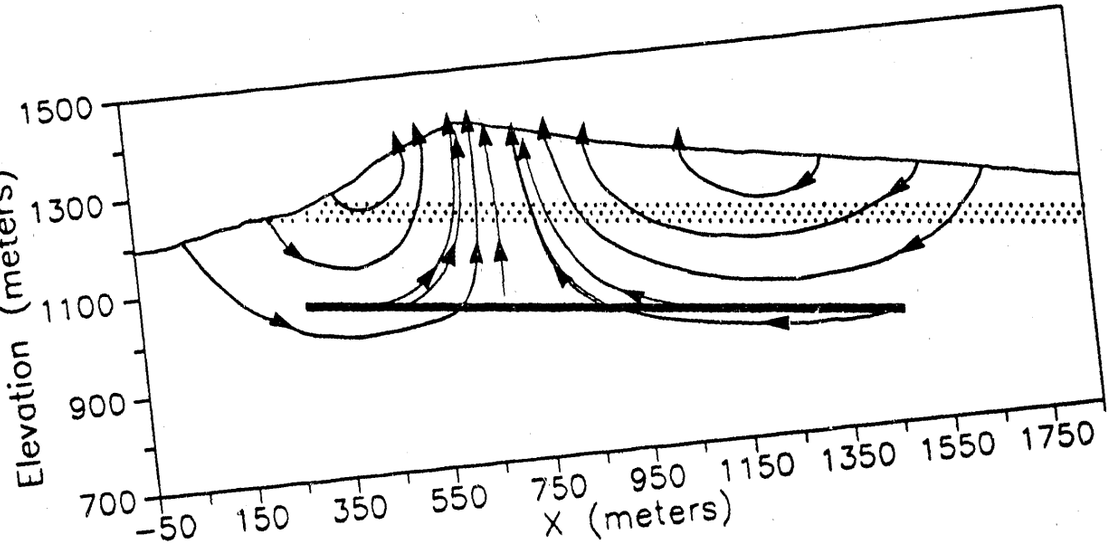

Figure 6b. Path lines with ambient temperature, no permeability contrast.

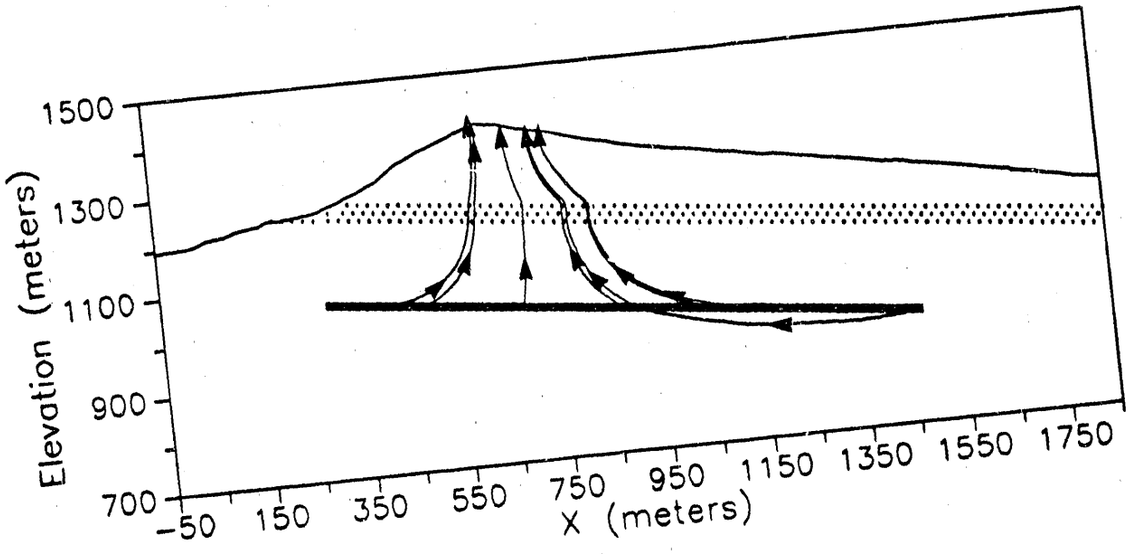

Figure 6c. Path lines with ambient temperature, 10× permeability contrast.

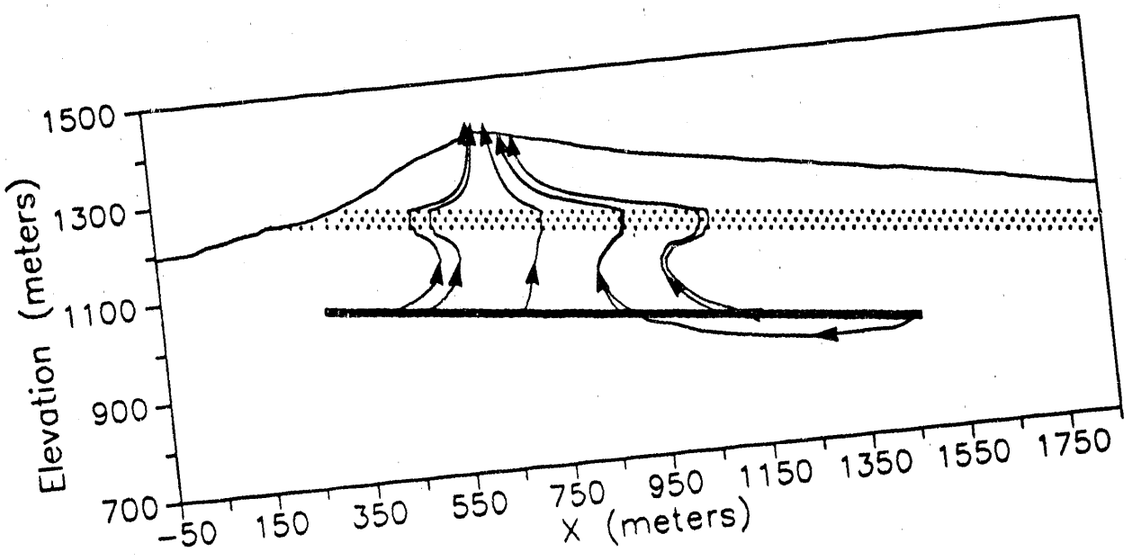

Figure 6d. Path lines with ambient temperature, 100× permeability contrast.

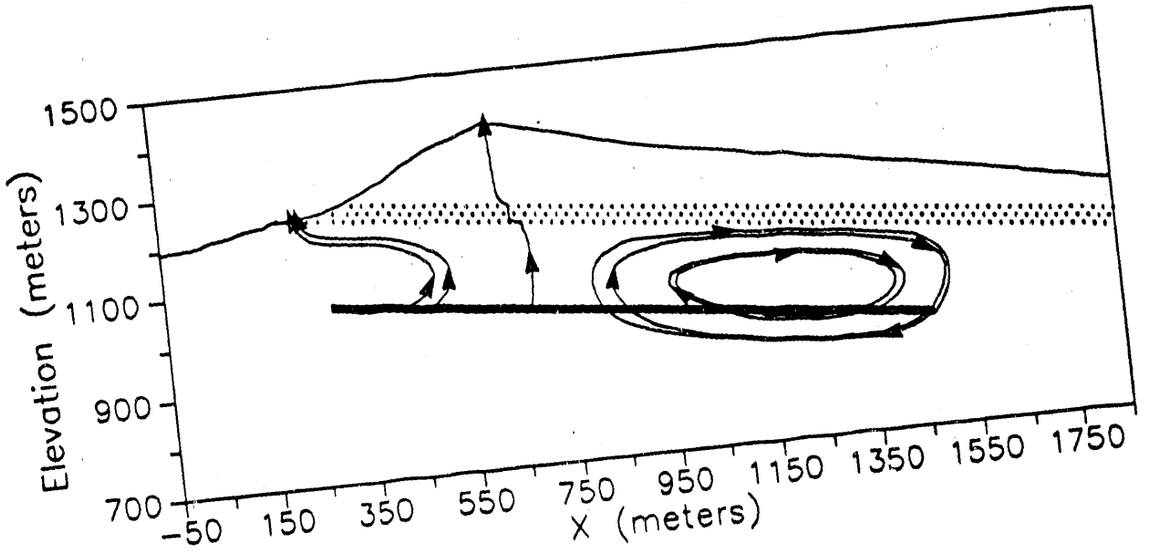

Figure 6e. Path lines with ambient temperature, 1000× permeability contrast.

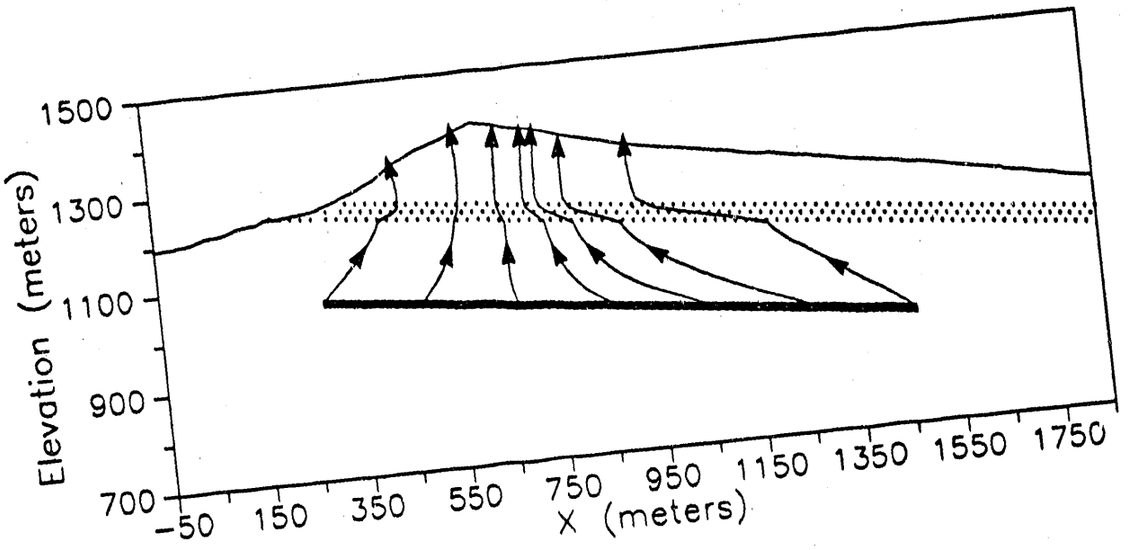

Figure 7a. Path lines with the repository heated to 330 K, 0.1× permeability contrast.

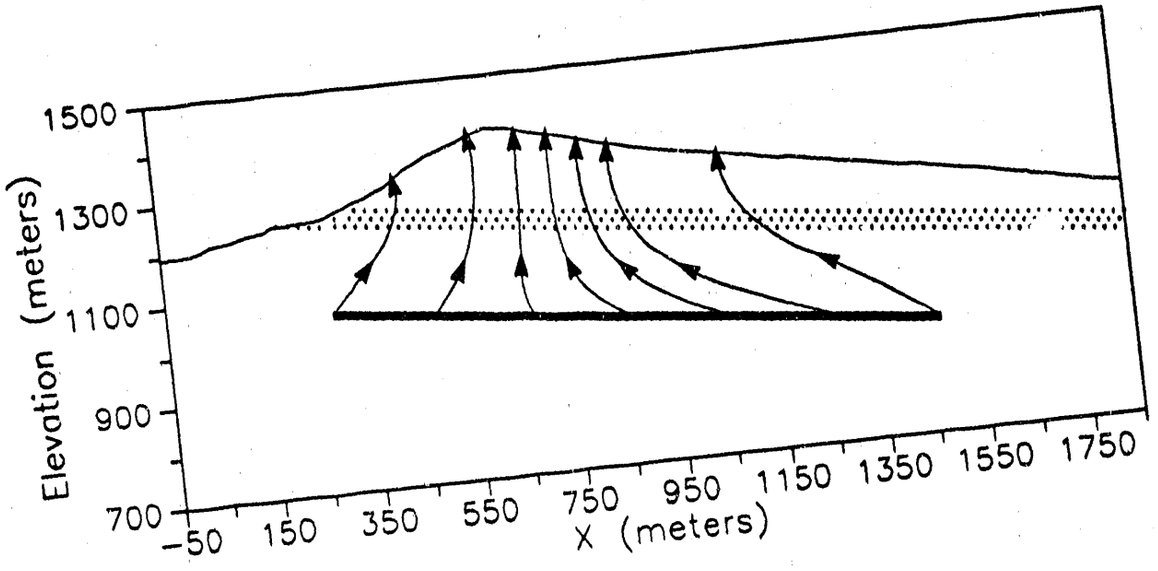

Figure 7b. Path lines with the repository heated to 330 K, no permeability contrast.

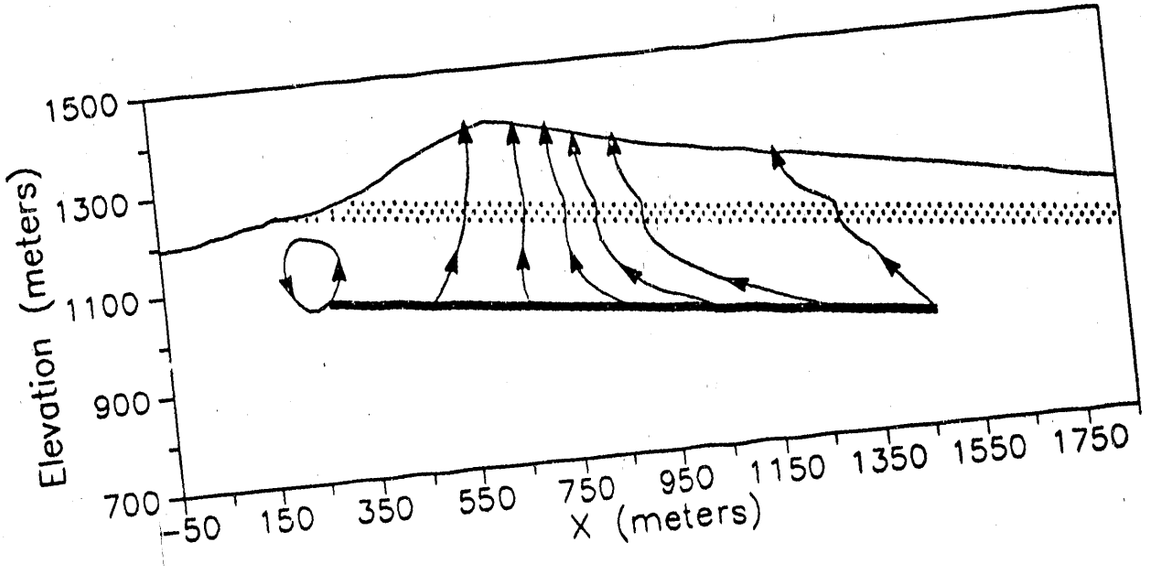

Figure 7c. Path lines with the repository heated to 330 K, 10× permeability contrast.

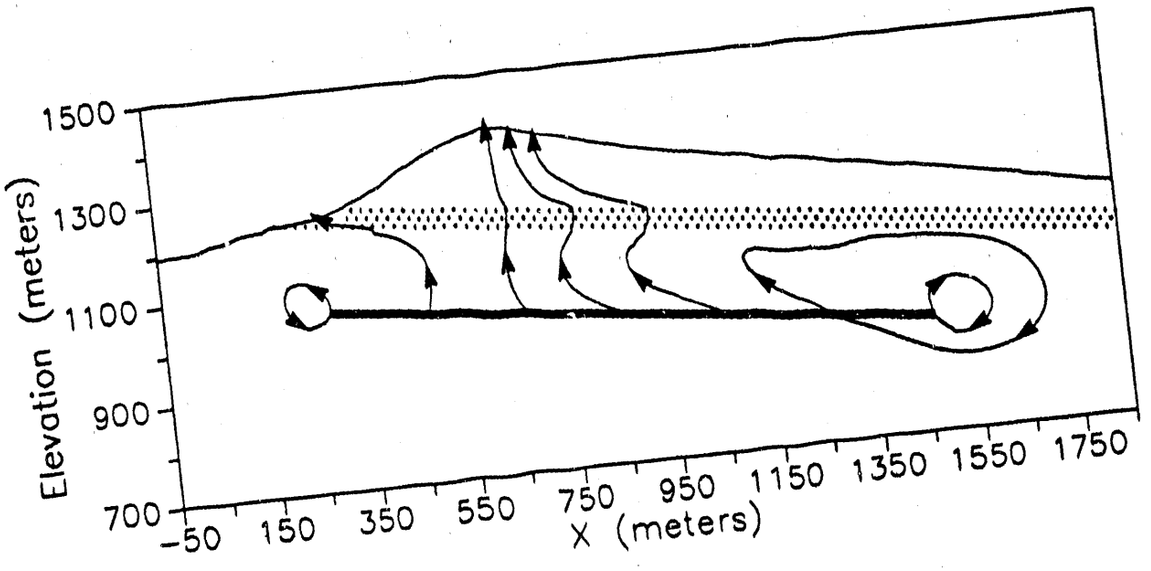

Figure 7d. Path lines with the repository heated to 330 K, 100× permeability contrast.

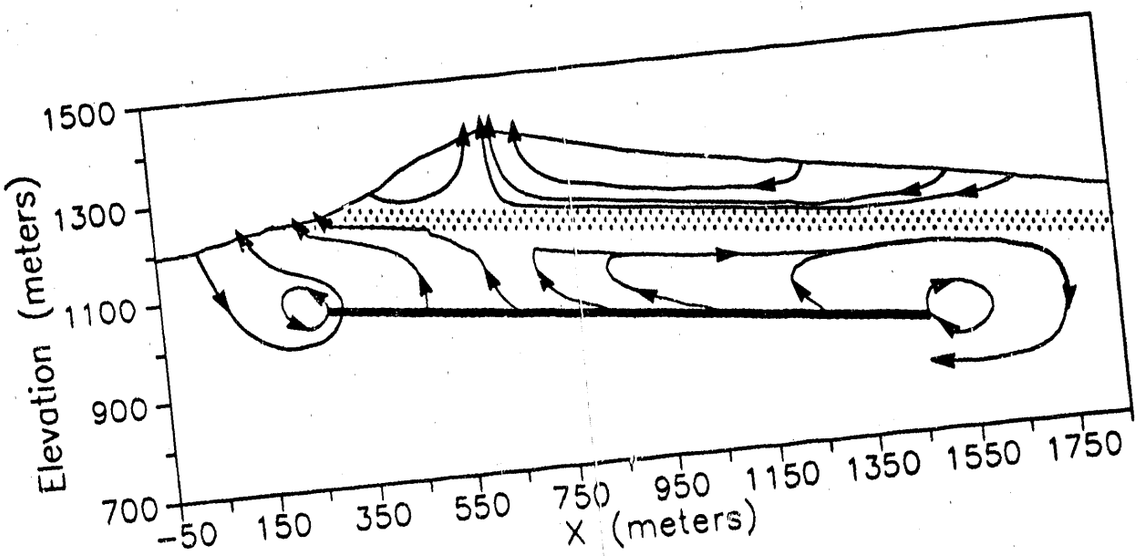

Figure 7e. Path lines with the repository heated to 330 K, 1000× permeability contrast.

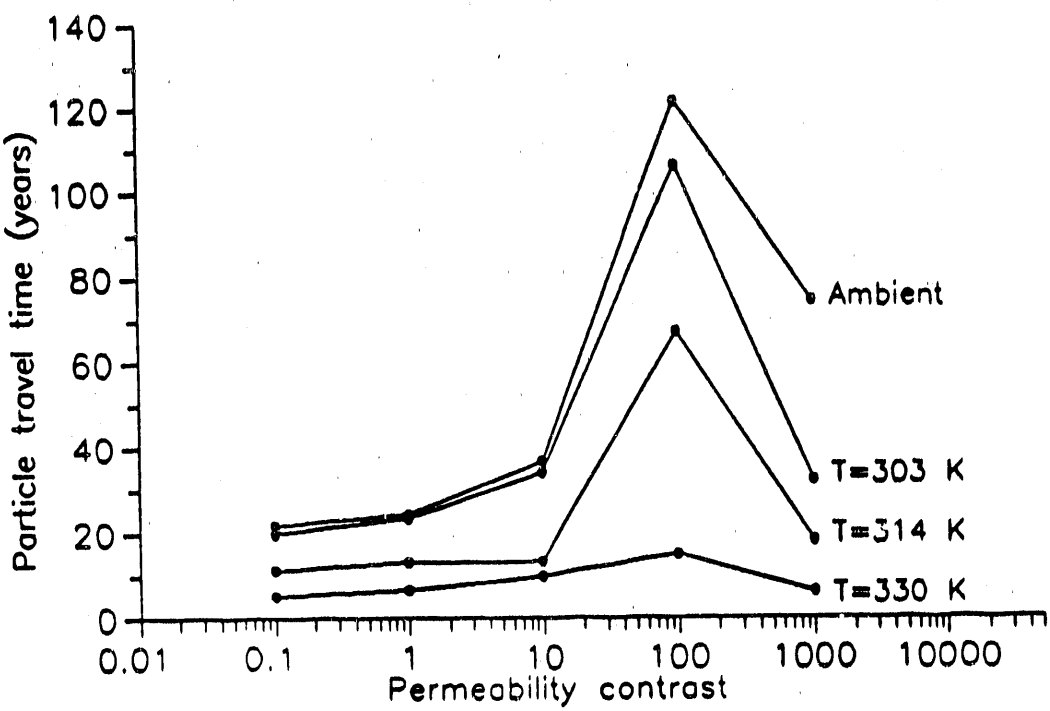

Figure 8. The minimum particle travel time from the repository as a function of the permeability contrast.

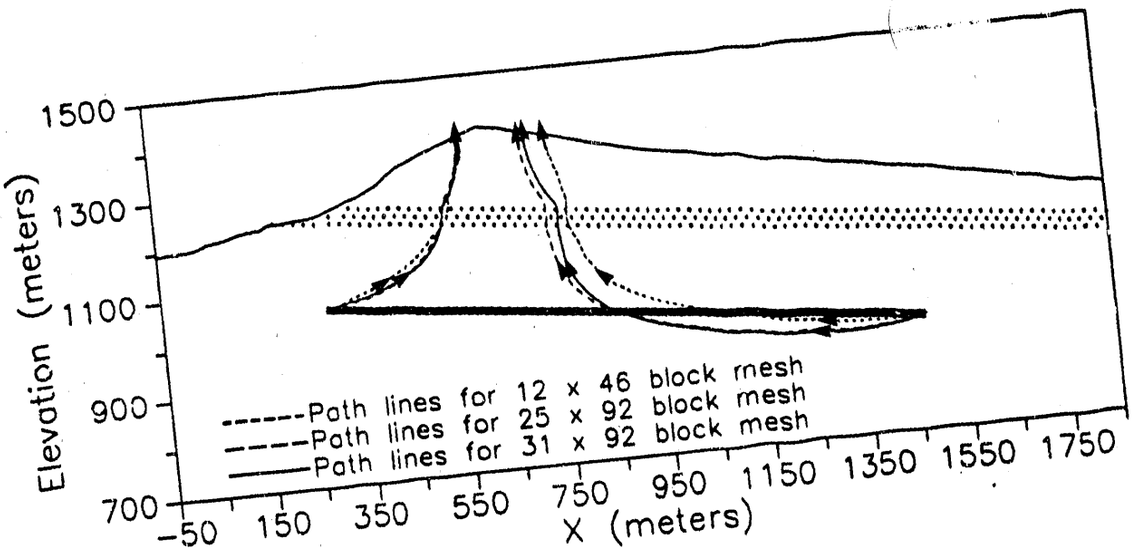

Figure 9. Comparison of path lines for different mesh densities with the repository heated to 303 K, 10 permeability contrast.

Appendix

Information from the Reference Information Base Used in this Report

This report contains no information from the Reference Information Base.

Candidate Information for the Reference Information Base

This report contains no candidate information for the Reference Information Base.

Candidate Information for the Site & Engineering Properties Data Base

This report contains no candidate information for the Site and Engineering Properties Data Base.

END

DATE FILMED

03/05/91